PARAMETER IDENTIFICATION FOR SOIL SIMULATION BASED ON THE DISCRETE ELEMENT METHOD AND APPLICATION TO SMALL SCALE SHALLOW PENETRATION TESTS

Jonathan Jahnke[1,*], Stefan Steidel[1], Michael Burger[1], Salomi Papamichael[2], Andreas Becker[2] and Christos Vrettos[2]

[1] Department Dynamics, Loads and Environmental Data
Division of Mathematics for Vehicle Engineering
Fraunhofer Institute for Industrial Mathematics ITWM
Fraunhofer-Platz 1, 67663 Kaiserslautern, Germany
e-mail: [jonathan.jahnke, stefan.steidel, michael.burger]@itwm.fraunhofer.de

[2] Division of Soil Mechanics and Foundation Engineering
Technical University Kaiserslautern
Erwin-Schrödinger-Straße, 67663 Kaiserslautern, Germany
e-mail: [salomi.papamichael, andreas.becker, christos.vrettos]@bauing.uni-kl.de

Key words: Granular Materials, Discrete Element Method, Parametrization, Triaxial Compression Test, Shallow Penetration Test

Abstract. The Discrete Element Method (DEM) is well-established and widely used in soil-tool interaction related applications. As for all simulation tools, a proper calibration of the model parameters is crucial. In this contribution, we present the parametrization procedure of the DEM software *GRAnular Physics Engine* (GRAPE), developed and implemented at Fraunhofer ITWM, and attempt to use two parametrized soil samples for the simulation of small scale shallow penetration tests. The results are compared to laboratory measurements.

1 Introduction

In recent years, the Fraunhofer ITWM has developed and implemented a software solution entitled *GRAnular Physics Engine* (GRAPE) for modeling and simulating soil and soil-tool interaction based on investigations in [1, 2, 3]. GRAPE is based on the Discrete Element Method (DEM) with a focus on the accurate prediction of draft forces with heavy construction equipment. The particles are represented by three-dimensional rigid spheres with three translational degrees of freedom and scale-invariant linear particle interaction forces in which the corresponding parametrization is based on a triaxial compression test, see Section 2 and 3. In particular, GRAPE is validated in real application scenarios among others in cooperation with Volvo Construction Equipment, cf. [4, 5].

The parametrization process for soil simulation is a challenging task. Cone penetrometer tests in the context of vehicle engineering have been studied in [6] using *Smoothed Particle Hydrodynamics*. Shallow hemiball and toroid penetrometers have been simulated using a *Large Deformation Finite Element Method* in [7] to find fitting equations for in situ evaluation and soil identification. Cone penetrometer tests, together with plate sinkage and shear tests have been used in an optimization routine to estimate DEM model parameters [8]. It was found that the combination of several in situ tests is sufficient for the calibration of their model. Small scale shallow penetration experiments using different materials have been conducted and evaluated in [9].

In this contribution, we illustrate the parameter identification process for two types of soil, namely a poorly graded sand (A) and a well graded sand-silt mixture (B) with mean grain diameter $d_{50}(A) = 0.290$ mm and $d_{50}(B) = 0.036$ mm, respectively. In Section 2 we describe the Discrete Element Method and explicate the specifics of our model. Thereafter, the experimental procedure on triaxial compression and shallow cone pentration test is shortly presented in Section 3. We determine the respective soil and particle interaction parameter sets $\mathcal{P}(A)$ and $\mathcal{P}(B)$ to match the observed strain-stress behavior in the corresponding triaxial compression tests, see Section 4. Subsequently, we discuss the applicability of these identified parameter sets – that reflect the triaxial test – to reproduce small scale shallow penetration tests performed in the soil mechanics laboratory, see Section 5. Finally, we summarize our results in Section 6.

2 Fundamentals of the DEM model

In this section, we briefly describe the Discrete Element Method in general and our efficient and soil-specific model in more detail [1, 10, 4, 11]. The DEM dates back to the 1970s [12] and with the rise of computing power as predicted by Moore's law, the method gained practical relevance in the 1990s until today. Zhu et al. [13] present a still ongoing boom referring to the number of particle simulation related publications. The main idea of the DEM is to consider soft-sphere particles and their interaction leading to granular bulk behavior. The decision on the shape of the particles and on how to model the inter particle contact law has to be taken with care. The physically most accurate contact law seems to be the Hertzian contact model with additions due to Mindlin and Deresievicz to account for cohesion [14]. Much more efficient but less physical is a linear-elastic Hookean model. However, when it comes to soil and granular matter with complex shapes, the error due to regularized geometries is much more relevant than the error owing to the linear contact law [15]. Due to the fact, that we are interested in the soil-tool interaction forces and usually do not focus on the micro-mechanical behavior of particle interaction, we choose the simplest geometry, namely spheres and a linear contact law. In our model, we neglect the rotational degrees of freedom, and solely rely upon an accurate parametrization in order to obtain physical bulk behavior, e.g. a realistic strain stress behaviour and angle of friction.

2.1 Normal interaction

The particle dynamics relies upon Newton's second law

$$m_i \ddot{\mathbf{x}}_i = \mathbf{f}_i. \tag{1}$$

Here m_i denotes the mass of the i-th particle, $\mathbf{x}_i$ its position, $\dot{\mathbf{x}}_i$ its velocity and $\ddot{\mathbf{x}}_i$ its acceleration vector. If two particles interact, that is the overlap $\delta_{ij} = r_i + r_j - \|\mathbf{x}_i - \mathbf{x}_j\|$ is non-negative, r_i denoting the radius of the i-th particle, a linear damped spring

$$F_{ij}^N = k_{ij}^N \delta_{ij} + d_{ij}^N \dot{\delta}_{ij} \qquad \text{and} \qquad \mathbf{f}_{ij}^N = F_{ij}^N \mathbf{n}_{ij}, \tag{2}$$

is activated. Here, the normal unit vector at the contact point is defined by

$$\mathbf{n}_{ij} = \frac{\mathbf{x}_i - \mathbf{x}_j}{\|\mathbf{x}_i - \mathbf{x}_j\|}.$$

The stiffness and damping coefficients k_{ij}^N and d_{ij}^N depend upon the particle radius.

Scale invariance and normal stiffness The terminology of scale-invariant contact laws is due to Feng [16]. Let us consider physical grains with radius r_P and larger model particles with radius r_M.

Definition 1 *We say that a model is scale-invariant, if and only if for radii r_P and r_M it holds $\sigma_P = \sigma_M$ for $\epsilon_P = \epsilon_M$.*

Lemma 1 *An n-dimensional contact law of the form $F = cr^\alpha \delta^\beta$ is scale-invariant if and only if $\alpha + \beta = n - 1$.*

This result is shown in [16]. Considering two particles as a stiff beam, with mean radius $r_{ij} = \frac{1}{2}(r_i + r_j)$ and mean area $A_{ij} = \pi r_{ij}^2$. The length of the beam corresponds to $L_{ij} = 2r_{ij}$. Considerung the normal stress σ and strain ε

$$\sigma = \frac{F_{ij}}{A_{ij}} = \frac{k_{ij}^N \delta_{ij}}{\pi r_{ij}^2} \qquad \text{and} \qquad \varepsilon = \frac{\delta_{ij}}{2r_{ij}}, \tag{3}$$

we obtain for the Young modulus

$$E_N = \frac{\sigma}{\varepsilon} = \frac{k_{ij}^N \cdot 2r_{ij}}{\pi r_{ij}^2} \qquad \text{thus} \qquad k_{ij}^N = \frac{E_N \pi r_{ij}}{2} \tag{4}$$

Hence the presented model, neglecting the damping term, describing a 3-dimensional contact law with $n = 3$ and $\alpha = \beta = 1$, is scale-invariant.

Normal Damping Furthermore, we set the inter-particle damping

$$d_{ij}^N = D_N \cdot 2 \cdot \sqrt{k_{ij}^N m_{ij}}, \qquad \text{where} \qquad m_{ij} = \frac{m_i \cdot m_j}{m_i + m_j}. \tag{5}$$

The effective mass m_{ij} stems from the consideration of two particles as one damped oscillator. The parameter D_N controls the desired percentage of the critical damping.

2.2 Tangential interaction

If two particles overlap, the initial contact points $\mathbf{c}_i = \mathbf{c}_j$ coincide and are saved in local coordinates of particle i and j. If the particles translate with respect to each other, the local contact points differ. We project them into the tangential contact plane and consider the resulting vector $\boldsymbol{\xi}_{ij}$ as tangential elongation. The tangential spring then reads

$$\mathbf{f}_{ij}^T = -k_{ij}^T \boldsymbol{\xi}_{ij} - d_{ij}^T \dot{\boldsymbol{\xi}}_{ij} \qquad \text{and} \qquad F_{ij}^T = \|\mathbf{f}_{ij}^T\|. \tag{6}$$

The parameters k_{ij}^T and d_{ij}^T are defined similarly to the normal interaction.

2.3 Coulomb friction

If the tangential elongation becomes large, we need to account for friction. We don't distinguish sticking and sliding friction and use the Coulomb friction model. We restrict the absolute value of the tangential force with respect to the normal force introducing the local stiffness parameter μ, that is $F_{ij}^T \leq \mu F_{ij}^N$. Otherwise slipping friction occurs and we reset the tangential elongation to

$$\boldsymbol{\xi}_{ij}' = \frac{\mu F_{ij}^N}{k_{ij}^T \|\boldsymbol{\xi}_{ij}\|} \boldsymbol{\xi}_{ij}. \tag{7}$$

3 Relevant experiments

We shortly describe the experimental setup of the triaxial compression test, needed for parameter identification. Thereafter, we focus on the small scale shallow penetration test.

3.1 Triaxial compression test

The triaxial compression test is a well-established laboratory test which has been developed in the first half of the 20th century. It serves as a method to quantify a material's strain-stress characteristic. For this study, displacement-controlled triaxial tests are carried out according to the specifications of DIN 18137. Dry samples of 100 mm in diameter and 120 mm in height are prepared using a standardized procedure. Confining pressure in the triaxial cell is applied using water in order to allow measurement of specimen volume change. Axial load is measured outside the cell. Piston friction is assessed by a calibration procedure. Volumetric strain is determined by measuring the volume change of the water in the triaxial cell from the differential movement of a piston. Strains are defined positive in compression. Loading of the sample is applied at a constant displacement rate of 0.1 mm/min. The variation of the axial load and of the volumetric strain are recorded at gradually increasing axial strain. Assuming a linear Mohr–Coulomb failure criterion, the shear strength parameters of the soil, i.e. angle of internal friction ϕ and cohesion c, are determined from the peak values of the strain-stress curves at three distinct levels of the cell pressure.

Two materials (A) and (B) are tested. They are classified as sand and sandy-silt, respectively. The porosity of the samples amounts to $n_A = 0.34 - 0.48$ for (A) and $n_B = 0.45 - 0.60$ for (B). The shear strength parameters, namely the angle of friction ϕ

and the amount of cohesion c for sand (A) and silt (B) as determined from the tests amount to $\phi_A = 39.5°, c_A = 2.1$ kPa and $\phi_B = 42.5°, c_B = 0.5$ kPa. For the parametrization we use the entire stress vs. strain and volume change vs. strain curves obtained from the tests as depicted in Figure 4.
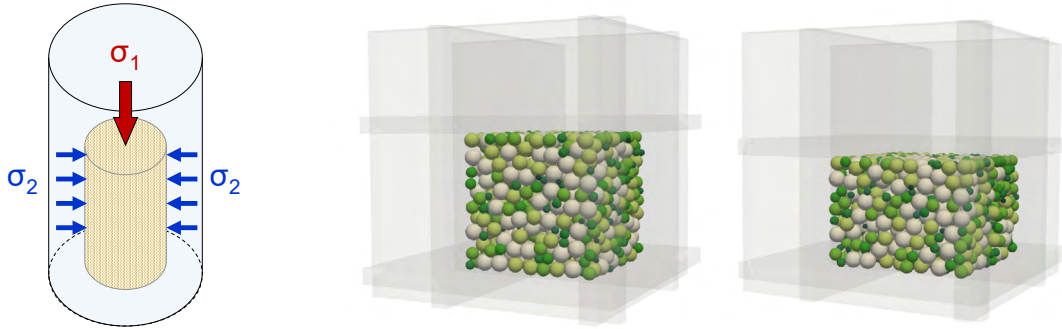
Figure 1: Visualization of the Triaxial Compression Laboratory Test (left) and the respective simulation at the beginning (middle) and in the end (right)

3.2 Shallow penetration test

The tests are carried out in a cylindrical container of a diameter of 290 mm and a height of 200 mm with a steel rod penetrometer of 10 mm diameter with a flat base. During the test, the penetration force and the corresponding displacement are measured for a total depth of 30 mm. The shallow penetration test is performed under a constant displacement rate of 1.2 mm/min. The force needed to penetrate the bar is continuously recorded by an appropriate load cell.
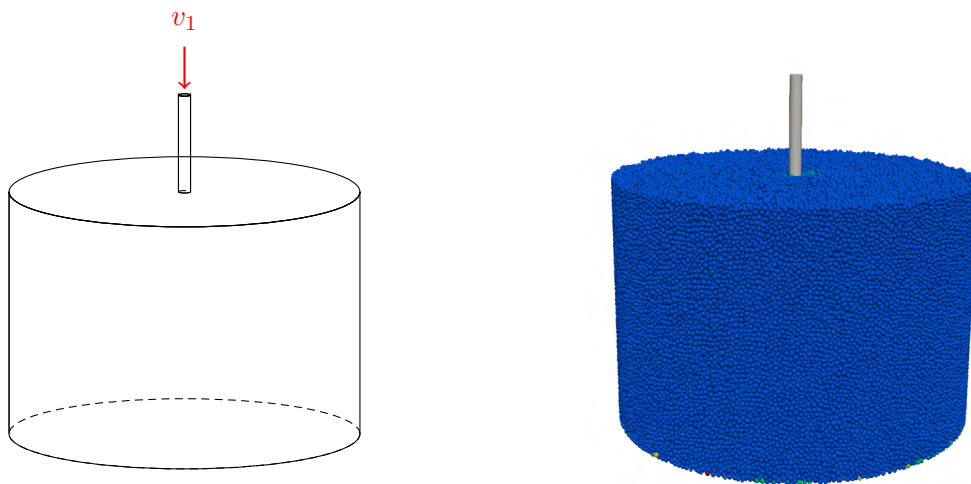
Figure 2: Visualization of the shallow cone penetration experiment and the respective simulation

Parameter	Symbol	Unit	sand $\mathcal{P}(A)$	silt $\mathcal{P}(B)$
Sample generation				
radii	r_i	[mm]	2	0.5-2.5
porosity	n	[-]	0.34-0.53	0.37-0.54
density	ρ	[kg/m^3]	2650	2700
Triaxial compression test				
Young modulus	E_N	[N/m^2]	1.2e8	1.2e7
tangential stiffness parameter	E_T	[N/m^2]	1e8	1e7
local friction coefficient	μ	[-]	0.2	0.25

**Table 1**: Parameters $\mathcal{P}(A)$ and $\mathcal{P}(B)$ as determined for the two materials

4 Parametrization via triaxial compression test

In this section, we describe the calibration procedure of our DEM model, as developed in [1, 10]. The parametrization of a GRAPE model is based on a triaxial test, see also Section 3, and implies the appropriate choice of the most influencing simulation parameters. First of all, we decide for the particle size distribution r_i that may represent a scaling of the real grain-size distribution due to the scale-invariant force law, see Section 2.1. The model parameters are the porosity n, the normal stiffness E_N and damping D_N, the tangential stiffness E_T and damping D_T and the local friction coefficient μ. The parameters of the virtual experiment are determined to reflect the soil's characteristic strain-stress behavior in the corresponding real experiment performed in the soil mechanics laboratory.

4.1 Sample generation

In a first step, we study the grain-size distribution and decide for suitable particle radii. Due to the scale-invariance, it is possible to use larger particles which reduces the simulation time, but limits the micro-mechanical modeling fidelity. The first choice is a monodisperse particle sample, which also simplifies the numerical calculation, because the particle stiffness and damping remain constant for all particles. The porosity of the material has to be estimated from the experimental minimal and maximal values. The particle density, corresponding to the mass equals to the density of the soil grain and can be measured in laboratory experiments. A list of all relevant parameters with the determined parameters for sand and silt is given in Table 1.

According to the desired grain-size distribution, the particles are loosely assembled on a regular lattice and slightly disturbed in a random direction. Thereafter, outer sidewalls compress the particles until the desired porosity is reached. This basic sample can then be replicated and cut in order to obtain a desired particle pile. For our study, we use mono-disperse particles of radius 2 mm for the poorly graded material (A). For the sandy-silt (B), we try to approximate the grain-size distribution using seven different particle radii between 0.5 and 2.5 mm, see Figure 3. The porosity of the material's basic sample corresponds to $n_A = 0.34$ and $n_B = 0.37$ for the triaxial compression test. The porosity for silt is underestimated with respect to the measurements. We focussed on reproducing the
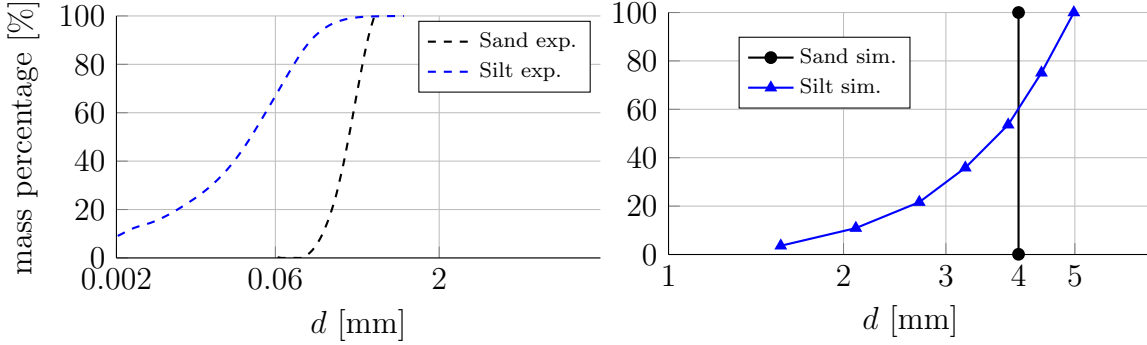
Figure 3: (left) Grain size distribution for two different materials: poorly graded sand (black) and well-graded sand-silt mixture (blue), which we denote by silt; (right) Particle size distribution within the simulation.

grain size distribution, which leads to a denser particle pile density. But when generating the cylindrical sample, we replicate the basic sample and consolidate it under the influence of gravity. The porosity then corresponds to $n_A = 0.53$ for material (A) and $n_B = 0.54$ for material (B).

4.2 Triaxial test simulations

The basic sample obtained in Section 4.1 is loaded in a triaxial test simulation. Instead of using a cylinder-shaped geometry, we use a cube, see Figure 1. The side-walls in horizontal and lateral direction are pressure-controlled. The bottom wall remains constant. The top wall is moved downwards at constant velocity, then the side-walls displace until an equilibrium between the desired side-wall pressure and the particles pressure is reached. The axial displacements ε_1, in vertical direction and ε_2 and ε_3 in horizontal and lateral direction, the volumetric strain ε_v and the top wall pressure σ_1 in vertical direction are recorded. Graphically, this leads to a strain-stress curve and a volumetric strain, axial strain curve, see Figure 4 and 5. The axial stress versus strain behavior demonstrates good accordance. The volumetric strain of silt behaves slightly different with respect to the simulation. The damping constants D_N and D_T are chosen as 0.1.

In this step, the stiffness and friction parameters are estimated. A useful concept is the stiffness number, which gives a rough estimate for the inter-particle stiffness [1]. Different authors have reported a connection between normal and tangential stiffness [17]. As discussed by Obermayr [10], we assume the ratio of $E_N/E_T = 1.2$. If a reasonable particle-particle stiffness yields good results within the triaxial compression test simulation, in terms of fitting the measured strain-stress relation for a specific side-wall pressure, we fine tune the strain-stress curves with the local stiffness constant μ. The parametrization may not be unique and is only valid in a certain pressure range.

5 Numerical results of shallow penetration test

First, we summarize the procedure to optimize the total time for the penetration simulation. The laboratory experiments are performed in a total time frame of about 25
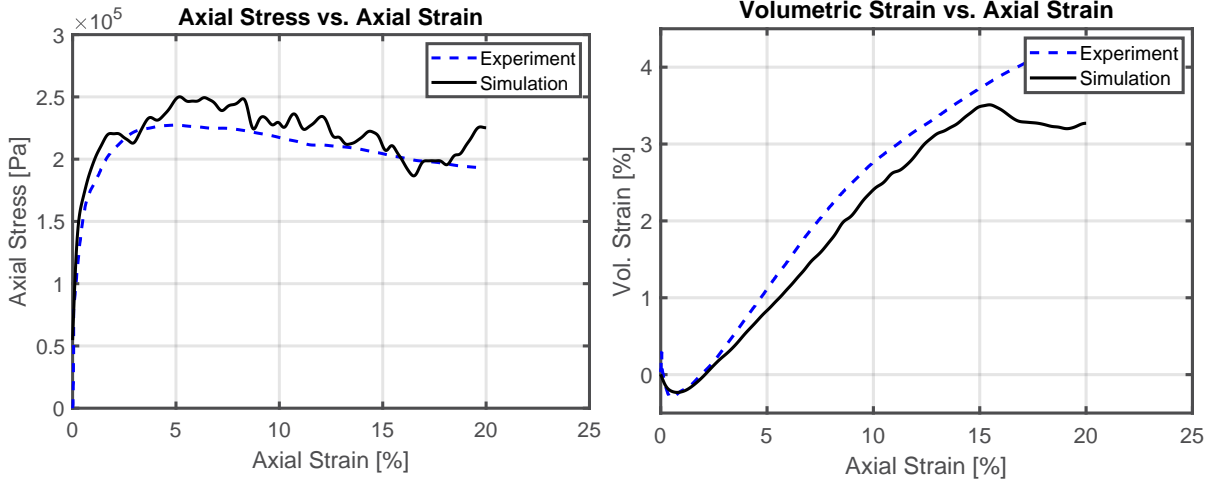
Figure 4: Simulation results of triaxial compression test and comparison to measurement for sand $\mathcal{P}(A)$, the side-wall pressure corresponds to $\sigma_2 = \sigma_3 = 50$ kPa.
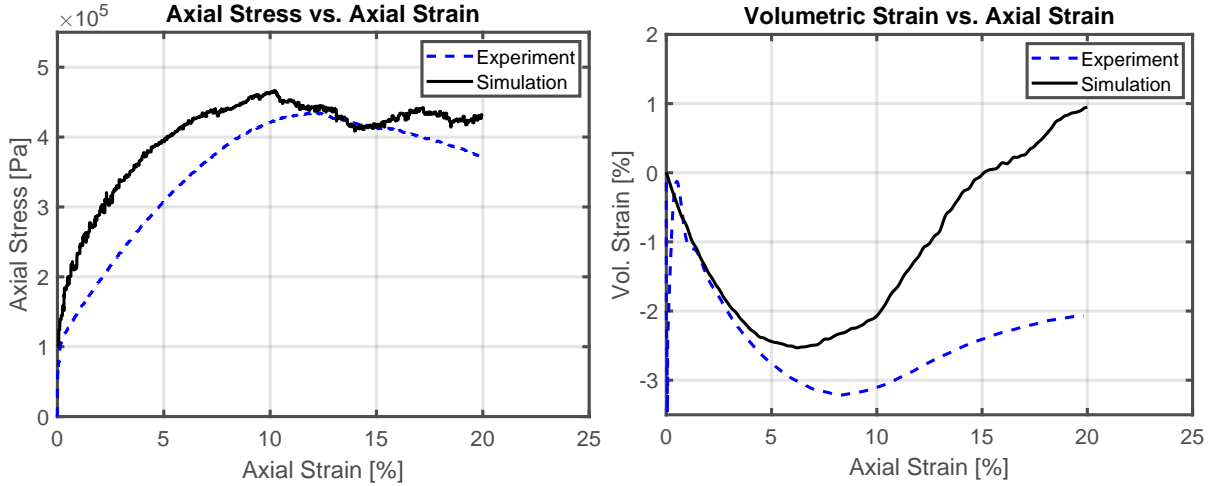
Figure 5: Simulation results of triaxial compression test and comparison to measurement for silt $\mathcal{P}(B)$, the side-wall pressure corresponds to $\sigma_2 = \sigma_3 = 80$ kPa.

minutes. This is not feasible in the simulation. We started with a simulation time of 30 to 60 seconds. As an estimate for the total time, we use the concept of the inertia number as introduced by [14] and [10]. More specifically, we consider the dimensionless number

$$I = 2\dot{\gamma}r\sqrt{\frac{\rho_g}{p}}, \tag{8}$$

where $\dot{\gamma}$ denotes the shear velocity, in our case we assume it to account for the amount of penetration distance per time, r the particle radius, ρ_g the density of the granular material and p the typical pressure. Da Cruz et al. [10, 18] report that the inertia number should not exceed 10^{-2} in order to remain in the quasi-static regime. The inertia number for our shallow penetration simulations suggest, that also smaller total time intervals lead to quasi-static simulations. The experimental time is in the range of 25 minutes, whereas

for the total simulation time we chose $t = 1$ s. Internal studies have shown that the simulation time does not seem to have a big influence on the total force output in vertical z-direction, working with quasi-static loads. Here, we simulate soil sample geometries of the same size as in the experiment, that is of height 200 mm and diameter of 290 mm. To save computation time it might be sufficient to have at least ten particles in each direction in order to obtain a good approximation of the bulk behavior. It should thus suffice to shrink the container, depending on the particle radius. We consider virtual soil samples for (A) and (B) with interaction parameters $\mathcal{P}(A)$ and $\mathcal{P}(B)$, simulate the corresponding penetration tests and compare the resulting particle reaction forces on the penetrator with the measured reaction forces in the experiment. The results show that
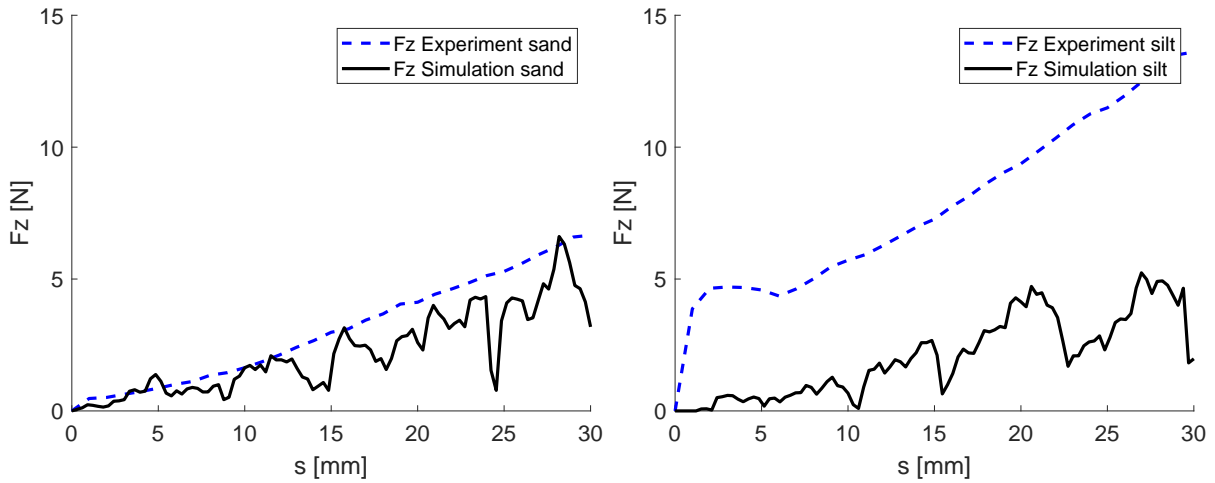
Figure 6: Force results with respect to the penetratration depth s of the shallow small scale penetration test; we obtain the penetration depth of 30 mm in a total simulation time of 1 second.

the reproduction of the observed behavior for the penetration in sand is satisfactory, see Figure 6 (left). In contrast, the simulated values for the indentation resistance in the silt-sand mixture are considerably lower than those observed in the tests. The latter show a sudden increase immediately after the start of the test, followed by a plateau and a monotonic increase in resistance. It seems that for this type of fine-grained material the DEM modeling is not capable in accurately reproducing both the triaxial compression test and the penetration test. Bear in mind that the shallow penetration of the flat-ended rod induces stress-singularity along the edge of the base contact area that considerably complicates matters. The unsteady nature of the simulated force reaction curve may arise because of the enlarged particle radii. The flat surface of the rod tip gives room for a limited number of particles. Each particle-tool interaction leads to a force jump. For large tool geometries such as plates and excavation tools, we expect some averaging effect, but for the small area of the rod, these impacts clearly influence the force output.

6 Discussion and conclusion

The procedure outlined in this presentation delivers a calibrated set of parameters that is validated on a boundary value problem. The force amplitude matches the result

obtained from the measurement on sand. The oscillations in the simulation results as shown in Figure 6, may be due to the larger particle radii. Thus only few particles collide with the tool which leads to unsteady force output.

The simulation underestimates the force response of the finer material. Here, our DEM model seems to have reached its limitations. Mainly three difficulties come into play. First, the fine-grained nature of silt is difficult to reproduce with the DEM. Scaling the grain-size distribution is challenging. Second, although the measured cohesion of $c_B = 0.5$ kPa is relatively low, it still maybe inaccurate to ignore it. And third, the surface effects of the shallow cone penetration test seem very difficult to model and the Discrete Element Method may not be able to capture this behavior.

The parametrization procedure relies upon simulation and careful selection of the interaction parameters. An automated procedure would be favorable. The collected data, generated during the simulation process may be used to find a good initial guess regarding future soil parametrizations.

Acknowledgement

REFERENCES

[1] Obermayr, M., Dressler, K., Vrettos, C. and Eberhard, P. Prediction of draft forces in cohesionless soil with the Discrete Element Method. *Journal of Terramechanics* (2011) **48(5)**:347–358.

[2] Obermayr, M., Dressler, K., Vrettos, C. and Eberhard, P. A bonded-particle model for cemented sand. *Computers and Geotechnics* (2013) **49**:299–313.

[3] Obermayr, M., Vrettos, C., Eberhard, P. and Däuwel, T. A discrete element model and its experimental validation for the prediction of draft forces in cohesive soil. *Journal of Terramechanics* (2014) **53**:93–104.

[4] Balzer, M., Burger, M., Däuwel, T., Ekevid, T., Steidel, S. and Weber, D. Coupling DEM Particles to MBS Wheel Loader via Co-Simulation . In *Proceedings of the 4th Commercial Vehicle Technology Symposium, Kaiserslautern* (2016):479–488.

[5] Burger, M., Dressler, K., Ekevid, T., Steidel, S. and Weber, D. Coupling a DEM material model to multibody construction equipment. In *Proceedings of the ECCOMAS Thematic Conference on Multibody Dynamics 2017* (2017):417–424.

[6] Goodin, C. and Priddy, J. D. Comparison of SPH simulations and cone index tests for cohesive soils. *Journal of Terramechanics* (2016) **66**:49–57.

[7] Stanier, S. A. and White, D. J. Shallow Penetrometer Penetration Resistance. *J. Geotech. Geoenviron. Eng.* (2015) **141(3)**:04014117.

[8] Asaf, Z., Rubinstein, D. and Shmulevich, I. Determination of discrete element model parameters required for soil tillage. *Soil and Tillage Research* (2007) **92(1)**:227–242.

[9] Vrettos, C., Becker, A., Merz, K. and Witte, L. Penetration Tests in a Mold on Regolith Quasi-Analogues at Different Relative Densities. In *Earth and Space 2014: Engineering for Extreme Environments* (2014):10–15.

[10] Obermayr, M. *Prediction of Load Data for Construction Equipment using the Discrete Element Method.* PhD thesis, Universität Stuttgart, Shaker Verlag (2013).

[11] Jahnke, J., Steidel, S., Burger, M. and Simeon, B. Efficient Particle Simulation Using a Two-Phase DEM-Lookup Approach. In *Proceedings of the ECCOMAS Thematic Conference on Multibody Dynamics 2019* (2019).

[12] Cundall, P. and Strack, O. A discrete numerical model for granular assemblies. *Geotechnique* (1979) **29**:47–65.

[13] Zhu, H., Zhou, Z., Yang, R. and Yu, A. Discrete particle simulation of particulate systems: Theoretical developments. *Chemical Engineering Science* (2007) **62(13)**:3378–3396.

[14] O'Sullivan, C. *Particulate Discrete Element Modelling.* CRC Press (2011).

[15] Renzo, A. D. and Maio, F. P. D. Comparison of contact-force models for the simulation of collisions in DEM-based granular flow codes. *Chemical Engineering Science* (2004) **59(3)**:525–541.

[16] Feng, Y., Han, K., Owen, D. and Loughran, J. On upscaling of discrete element models: similarity principles. *Engineering Computations* (2009) **26(6)**:599–609.

[17] Belheine, N., Plassiard, J., Donze, F., Darve, F. and Seridi, A. Numerical simulation of drained triaxial test using 3D discrete element modeling. *Computers and Geotechnics* (2009) **36**:320–331.

[18] da Cruz, F., Emam, S., Prochnow, M., Roux, J.-N. and Chevoir, F. Rheophysics of dense granular materials: Discrete simulation of plane shear flows. *Phys. Rev. E* (2005) **72**:021309.